SUPPORTING INFORMATION

A Versatile Interfacial Co-Assembly Method for Fabrication of Tunable Silica Shells with Radially Aligned Dual Mesopores on Diverse Magnetic Core Nanoparticles

Sebastjan Nemec[†,‡] and Slavko Kralj[*,†,‡,‖]

† Department for Materials Synthesis, Jožef Stefan Institute, Jamova 39, 1000 Ljubljana, Slovenia

‡ Faculty of Pharmacy, University of Ljubljana, Aškerčeva cesta 7, 1000 Ljubljana, Slovenia

‖ Nanos SCI, Nanos Scientificae d.o.o., Teslova 30, 1000 Ljubljana, Slovenia

Corresponding Author

*E-mail: slavko.kralj@nanos-sci.com. Phone: 00386 1 477 3629. Fax: 00386 1 252 9385.

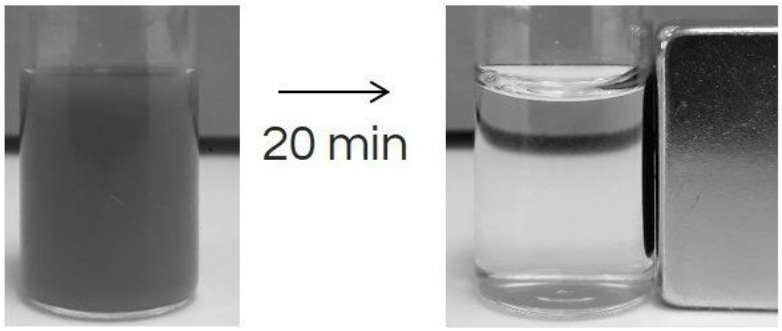

Figure S1. Demonstration of the magnetic responsiveness of the nanochains with radially aligned silica pores.

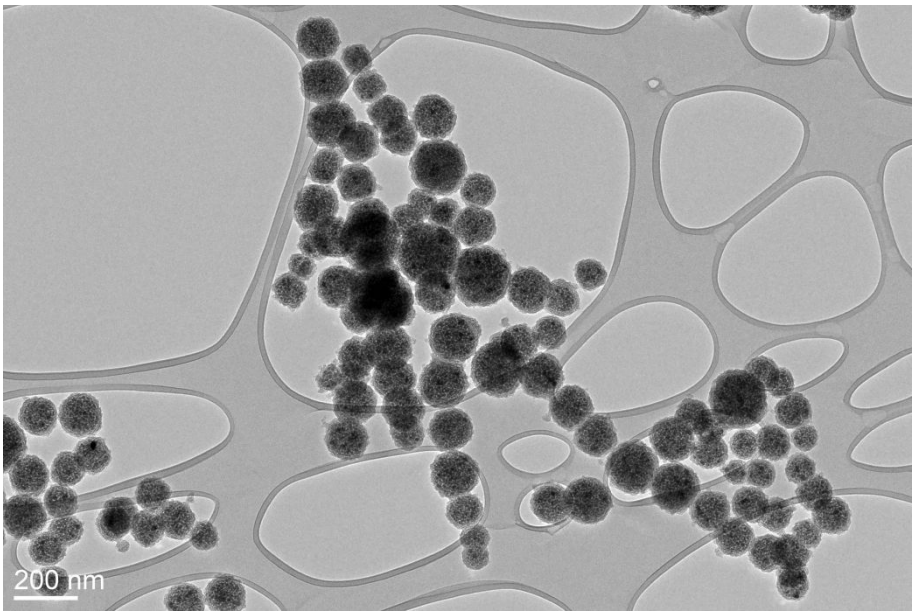

Figure S2. Representative transmission electron microscopy micrograph of magnetic nanochains coated with silica using the sodium dodecyl sulfate surfactant instead of the CTAB used for the general procedure reaction conditions. The silica was not

deposited on the surface of the core nanochains and the colloidal stability of the nanochains was impaired. Scale bar: as indicated.

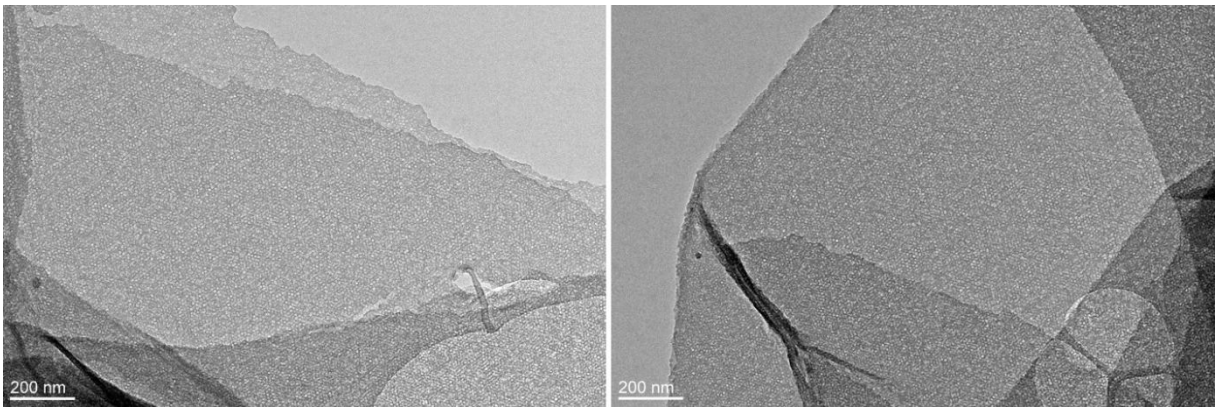

Figure S3. Representative transmission electron microscopy micrographs of planar silica sheets with holes at a micron-scale dimension. The material was synthesized as a by-product when the CTAB concentration of the general procedure was increased by two-fold. Scale bars: as indicated.

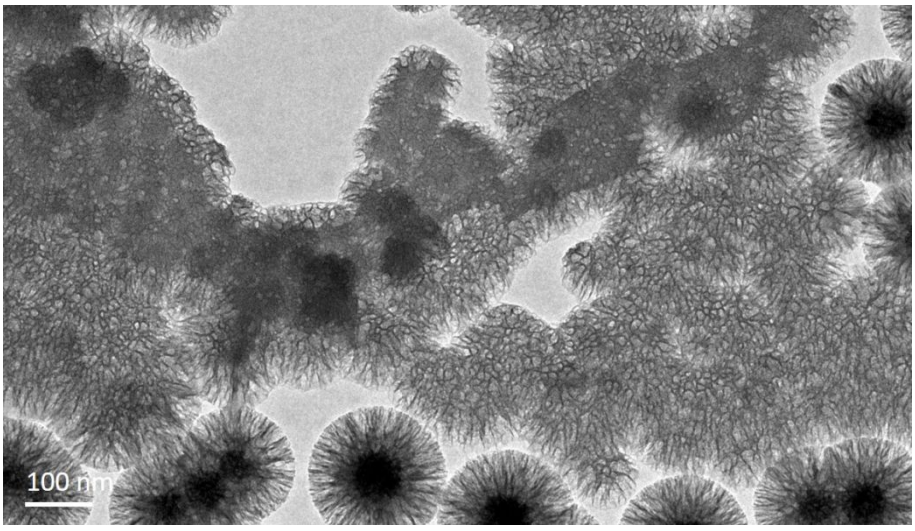

Figure S4. Representative transmission electron microscopy micrograph of undesired formless silica deposits. The material was synthesized as a by-product when the CTAB concentration of the general procedure was reduced by a factor of three. Scale bar: as indicated.

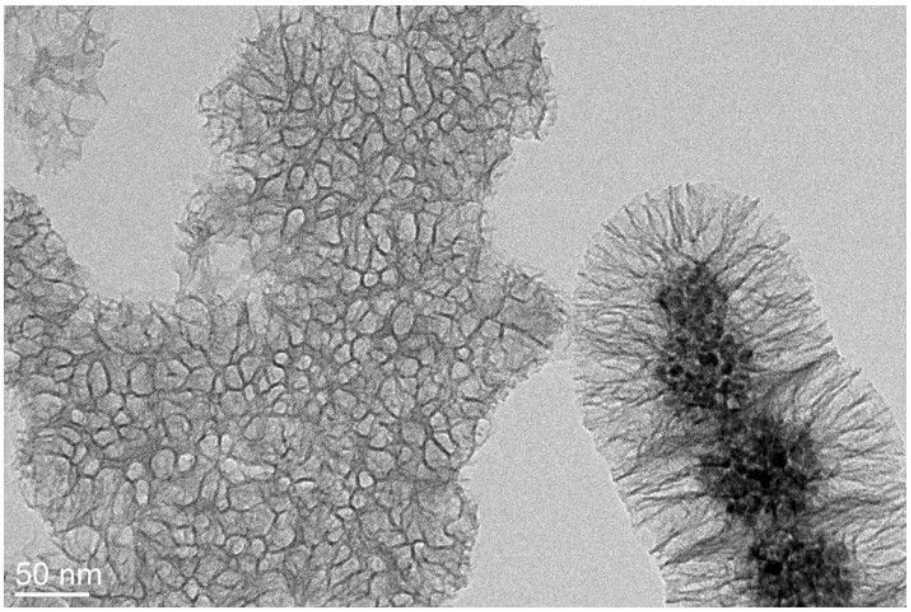

Figure S5. Representative transmission electron microscopy micrograph of undesired formless silica deposits. The material was synthesized as a by-product when the TEOS concentration of the general procedure was increased by three-fold. Scale bar: as indicated.

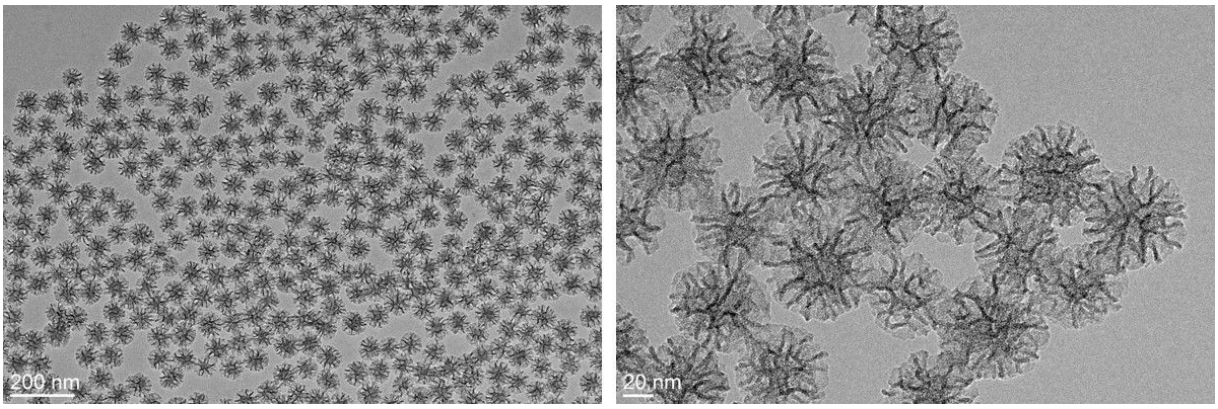

Figure S6. Representative transmission electron microscopy micrographs of monodispersed mesoporous silica nanoparticles with mean size of ~60 nm. These nanoparticles were formed when the TEOS concentration of the general procedure was increased by nine-fold. Scale bars: as indicated.

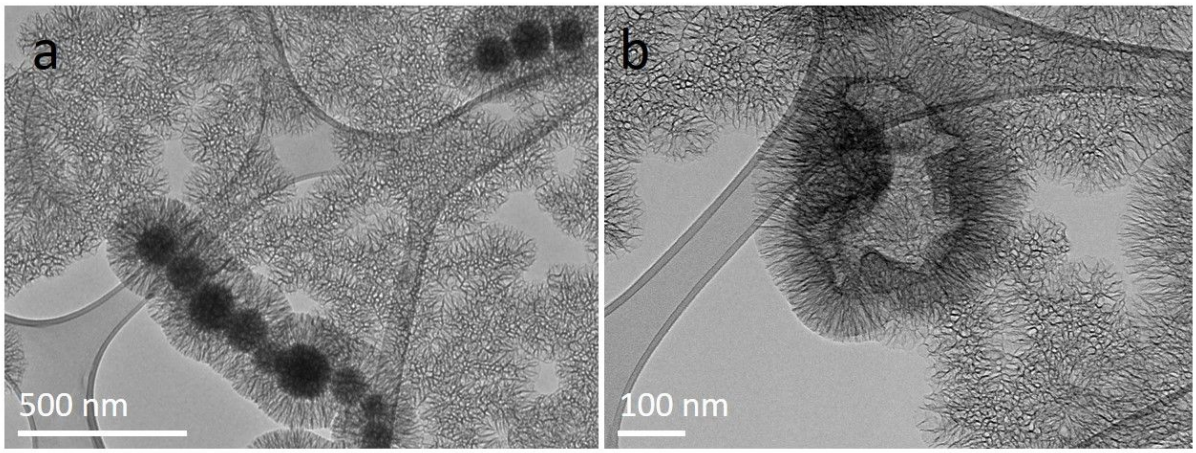

Figure S7. Representative transmission electron microscopy micrographs of undesired formless silica deposits. The materials were synthesized when (a) three-fold and (b) six-fold increases in the cyclohexane volumes compared to the general procedure were used. Scale bar: as indicated.

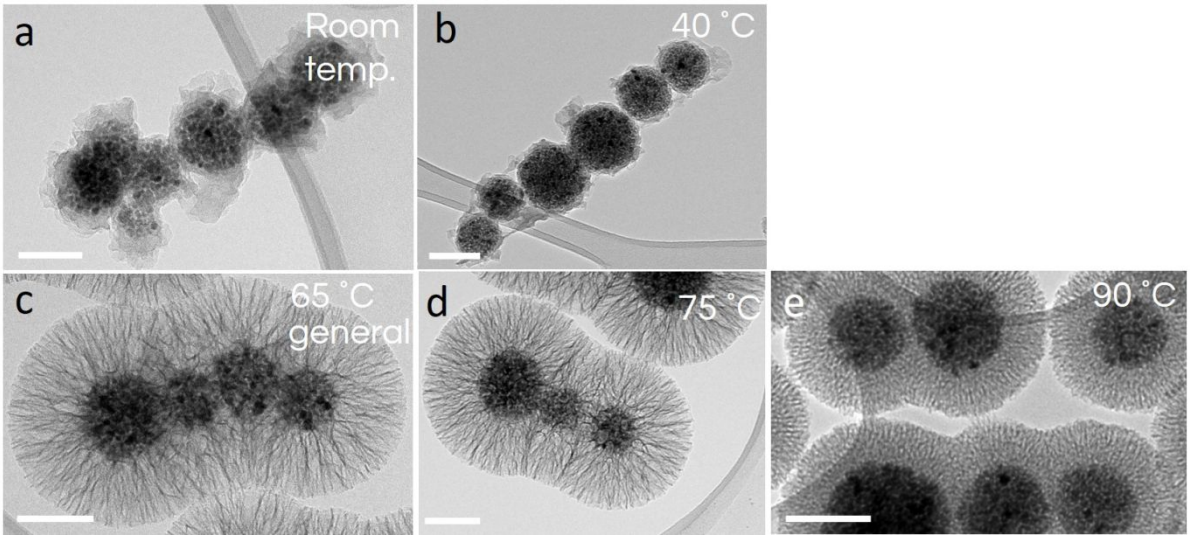

Figure S8. Representative transmission electron microscopy micrographs of core-shell magnetic nanochains with diverse silica-shell morphologies synthesized at various reaction temperatures: (a) room temperature. (b) 40 °C. (c) 65 °C. (d) 75 °C. (e) 90 °C. Scale bars: 100 nm.

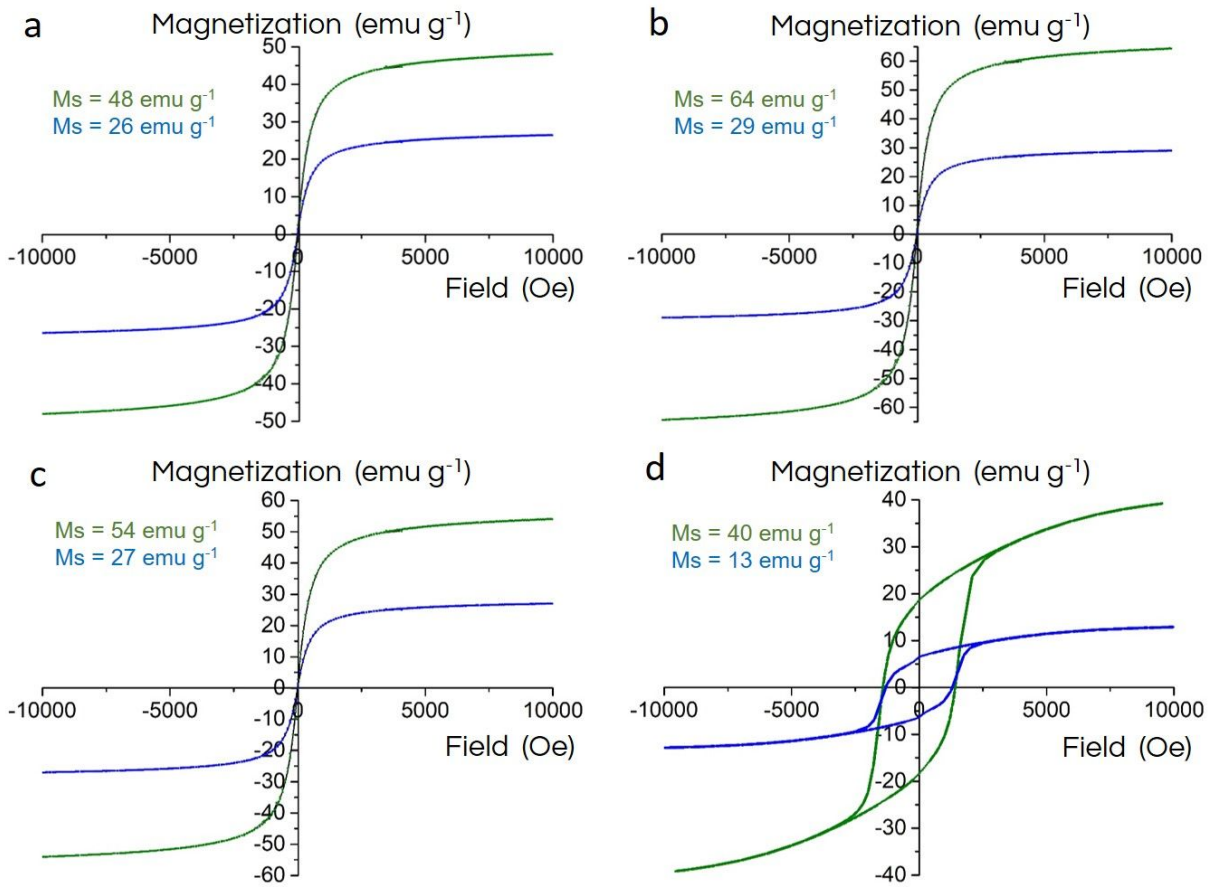

Figure S9. Room-temperature measurements of the mass magnetization as a function of magnetic field for the superparamagnetic nanochains (a), superparamagnetic iron oxide nanocrystals (SPIONs) (b), superparamagnetic nanoparticle clusters (c), and ferromagnetic hexaferrite nanoplatelets (d). Green color curves represent the samples measured before the coating with silica while the blue ones after the mesoporous silica coating. Saturation magnetization values were reduced after the silica coating due to its non-magnetic (diamagnetic) nature and were therefore 26 emu g^{-1}, 29 emu g^{-1}, 27

emu g^{-1}, 13 emu g^{-1} for the mesoporous samples of the nanochains, SPIONs, nanoparticle clusters and hexaferrites, respectively.

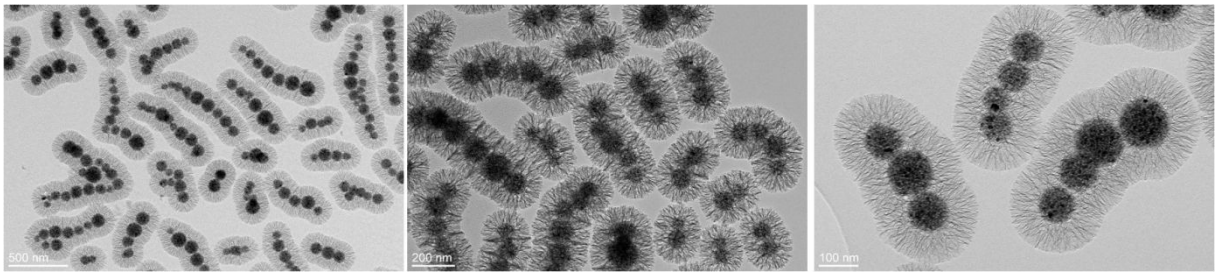

Figure S10. Representative transmission electron microscopy micrographs of the core-shell magnetic nanochains with radially aligned silica pores after exposure of the suspensions to strong 1-s-long ultrasound pulses (3 min total; volume, 10 mL; amplitude, 40 %; Sonics Vibra-Cell – VC505) following overnight drying at 80 °C.

Table S1. Effects of different amounts of the TEOS silica source compared to the general procedure, on the mesoporous silica shell thickness, pore size and extra silica nanoparticles.

Change in TEOS concentration	Extent of TEOS change	Stirring rate [rpm]	Mean shell thickness [nm][a]	Mean pore size [nm][b]	Extra silica nanoparticles
Reduction	Factor of 3	600	45	18	Absent
None	(General procedure)	600	~95	17	Absent
	(General procedure)	300[c]	Inhomogeneous reaction mixture		/
Increase	3-fold	600	90	16	Few (<5 %)
	3-fold	900[d]	90	16	Few (<2 %)

	9-fold	600	80	12	Substantial (>20 %)

[a)] Shell thickness was determined from transmission electron microscopy micrographs, with the shells of 100 particle measured
[b)] All nitrogen desorption followed Barrett–Joyner–Halenda analysis, with a sharp peak at ~3 nm to 4 nm, similar to Figure 2E
[c)] The stirring rate of 300 rpm resulted in an inhomogeneous reaction mixture where the separation of the cyclohexane phase from the aqueous phase was detected.
[d)] The stirring rate of 900 rpm resulted in an excessive foaming.

Table S2. Effects of type and volume of organic solvents as pore expanders compared to the general procedure, on the mesoporous silica-shell thickness and pore size.

Organic solvent	Change in organic solvent volume	Extent of volume change	Mean shell thickness [nm][a]	Mean pore size [nm][b]
None	No solvent added	-	25	Compact; no pores observed
Cyclohexane	Reduction	Factor of 6	25	5 (raspberry structure)
	None	(General procedure)	95	17
	Increase	3-fold	83	14
		6-fold	72	40
Hexane	None	-	40	14
Dibenzyl ether	None	-	83	18
Toluene	None	-	90	41
Ethyl acetate	None	-	-	-
	Reduction	Factor of 6	20	Compact; no pores observed

[a)] Shell thickness was determined from transmission electron microscopy micrographs, with the shells of 100 particle measured
[b)] All nitrogen desorption followed Barrett–Joyner–Halenda analysis, with a sharp peak at ~3 nm to 4 nm, similar to Figure 2E

Table S3. Effects of different catalysts (base) compared to TEOA as the general procedure, on mesoporous silica-shell thickness, pore size and extra silica nanoparticles.

Base	Mean shell thickness [nm][a]	Mean pore size [nm][b]	Extra silica nanoparticles
TEOA (general procedure)	95	17	Absent
TRIS	86	17	Absent
NH3	45	21	Substantial (>20 %)

TEA	38	19	Substantial (>20 %)
NaOH	20	Compact; no pores observed	Few (<5 %)

[a)] Shell thickness was determined from transmission electron microscopy micrographs, with the shells of 100 particle measured

[b)] All nitrogen desorption followed Barrett–Joyner–Halenda analysis, with a sharp peak at ~3 nm to 4 nm, similar to Figure 2E

Table S4. Effects of different TEOA catalyst amounts compared to the general procedure, on the mesoporous silica shell thickness, pore size and presence of extra silica NPs.

Change in TEOA	Extent of TEOA change	Mean shell thickness [nm][a]	Mean pore size [nm][b]	Extra silica nanoparticles
Reduction	Factor of 3	68	15	Absent
None	(General procedure)	95	17	Absent
Increase	3-fold	58	17	Absent
	6-fold	29	~31	Few (<5 %)

[a)] Shell thickness was determined from transmission electron microscopy micrographs, with the shells of 100 particle measured

[b)] All nitrogen desorption followed Barrett–Joyner–Halenda analysis, with a sharp peak at ~3 nm to 4 nm, similar to Figure 2E

Table S5. Effects of different temperatures compared to the 65 °C general procedure, on the mesoporous silica-shell thickness and pore size.

Temperature [°C]	Mean shell thickness [nm][a]	Mean pore size [nm][b]
Room temperature	-	-
40	-	-
65 (general procedure)	95	17
75	82	10
90	54	5 (raspberry structure)

[a)] Shell thickness was determined from transmission electron microscopy micrographs, with the shells of 100 particles measured

[b)] All nitrogen desorption followed Barrett–Joyner–Halenda analysis, with a sharp peak at ~3 nm to 4 nm, similar to Figure 2E